Extreme Mechanics Letters 51 (2022) 101610

Contents lists available at ScienceDirect

Extreme Mechanics Letters

journal homepage: www.elsevier.com/locate/eml

Electro-mechanical demultiplexer enabled by tunable electric circuits

Yanzheng Wang [a], Yongfeng Zheng [a,b], Mikhail V. Golub [c], Sergey I. Fomenko [c], Guoliang Huang [d], Weiqiu Chen [e,*], Chuanzeng Zhang [a,*]

[a] Chair of Structural Mechanics, Department of Civil Engineering, University of Siegen, 57068 Siegen, Germany
[b] Key Laboratory of Polymer Processing Engineering, Ministry of Education, Guangdong Provincial Key Laboratory of Technique and Equipment for Macromolecular Advanced Manufacturing, South China University of Technology, 510641 Guangzhou, China
[c] Institute for Mathematics, Mechanics and Informatics, Kuban State University, 350040 Krasnodar, Russia
[d] Department of Mechanical and Aerospace Engineering, University of Missouri, 65211 Columbia, MO, USA
[e] State Key Lab of CAD & CG, Key Laboratory of Soft Machines and Smart Devices of Zhejiang Province & Department of Engineering Mechanics, Zhejiang University, 310027 Hangzhou, China

ARTICLE INFO

Article history:
Received 19 November 2021
Received in revised form 26 December 2021
Accepted 6 January 2022
Available online 12 January 2022

Keywords:
Acoustic demultiplexer
Piezoelectric metamaterial plates
Shunting LC circuits
Highly tunable bandgaps

ABSTRACT

Inspired by the electronic demultiplexer, acoustic/elastic demultiplexers have received much attention in recent years. An acoustic/elastic demultiplexer can split one input wave signal into several output wave signals based on their frequencies. However, little to no work has been reported on the acoustic/elastic demultiplexers by considering the electro-mechanical coupling. In this letter, a multi-channel demultiplexer is proposed based on one-dimensional piezoelectric metamaterial plates connecting with shunting circuits. In particular, a four-channel electro-mechanical demultiplexer consisting of three electrically connected plates is constructed. As an outstanding example, the electro-mechanical wave with a certain frequency could propagate along a desired path. The underlying design principle relies on the indispensable character of the bandgaps of the piezoelectric plates, which are highly tunable by the external LC circuits. A numerical simulation is carried out by the two-dimensional spectral element method to validate the feasibility of the four-channel demultiplexer. Similarly to crystal filters or crystal oscillators, the proposed electro-mechanical demultiplexer could be integrated into some electronic devices, which may provide a wide range of applications in wireless telecommunication and electric signal processing.

1. Introduction

Phononic crystals and acoustic/elastic metamaterials are artificial materials or structures, whose material properties and/or geometries generally vary periodically in the space. Their outstanding capacity for the control of acoustic/elastic waves has received much research interest [1,2]. Some unprecedented acoustic/elastic wave phenomena or novel acoustic wave devices have been realized based on phononic crystals or acoustic/elastic metamaterials, such as negative refraction [3], unidirectional propagation [4], focusing [5], wave filtering [6], sensors [7], waveguides [8], superlens [9], cloaking [10], etc. Bandgaps are one of the most important properties of such materials, in which the wave propagation is prohibited. The bandgaps induced by Bragg scattering are referred to as the Bragg bandgaps due to the periodic variation of acoustic impedance. The bandgaps generated by local resonances of the unit-cell are called the resonance bandgaps.

The bandgaps are often unchangeable in the conventional phononic crystals or acoustic metamaterials after they are designed and manufactured, which may limit their practical applications. To overcome this limitation, some efforts have been made to achieve the tunable bandgaps by making use of the pre-deformation [11,12], the multi-field coupling [13–15], etc.

Electronic demultiplexer is a combinational logic circuit or switch, which can split one input signal into several signals outputting from different channels. Inspired by this, the researches on acoustic/elastic demultiplexers have flourished as the development of phononic crystals and acoustic metamaterials in recent years. The acoustic/elastic demultiplexers can split one multi-frequency wave signal into several single-frequency wave signals outputting from different channels, see Fig. 1b. It was proven that the acoustic/elastic waves can be guided into different output channels based on their frequencies by introducing the appropriate line or point defects into a phononic crystal [16–20]. In addition, the parallel connection of phononic crystals with the tunable band structures was also adopted to design the elastic/acoustic demultiplexers, in which the waves with the specific

* Corresponding authors.
E-mail addresses: chenwq@zju.edu.cn (W. Chen), c.zhang@uni-siegen.de (C. Zhang).

https://doi.org/10.1016/j.eml.2022.101610
2352-4316/

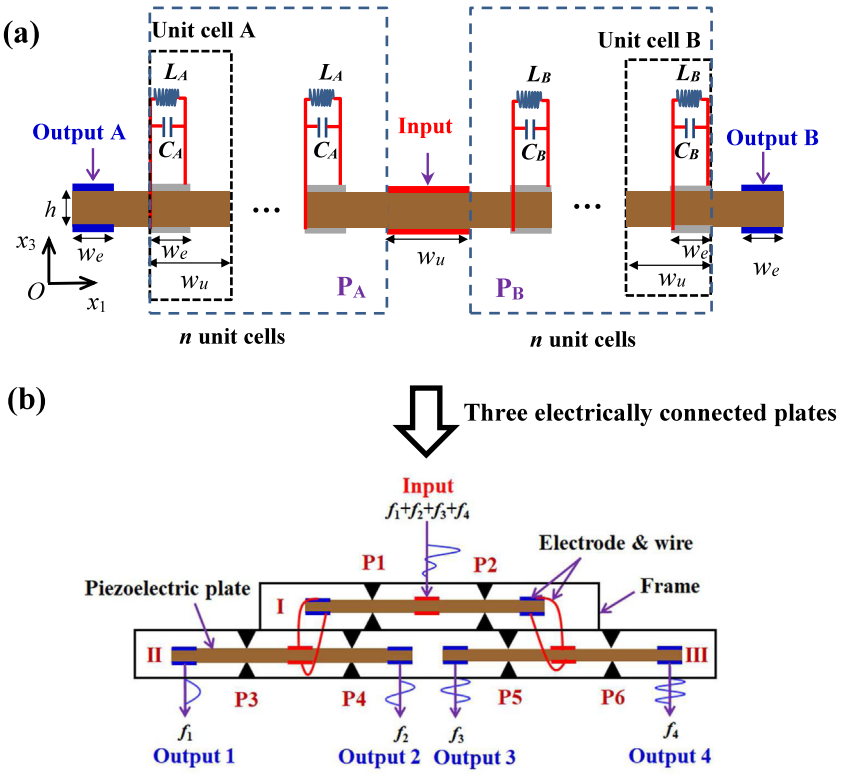

Fig. 1. The schematic illustration of the electro-mechanical demultiplexer. (a) The piezoelectric plate attached symmetrically with an array of periodic electrodes connected by the LC circuits, (b) the conceptual illustration of the 4-channel electro-mechanical demultiplexer made of three electrically connected piezoelectric plates. The three piezoelectric plates (plates I, II, III) are the same except the magnitudes of the inductances and the capacitances, and are connected by the wires. The circuits for the regions P1–P6 are shown in P_A and P_B.

frequencies can only transmit along the target routes [21,22]. To the knowledge of the authors, until now there is no report on elastic/acoustic demultiplexers with the electro-mechanical coupling, which however may further broaden their practical applications. Actually, the acoustic wave devices based on electro-mechanical materials have already obtained huge applications in a wide range. For example, crystal filters [23,24] and surface acoustic wave filters [25] were both developed based on piezoelectric materials, which play a particularly important role in the development of narrow-band communication systems and today's highly complex electronic products. Piezoelectric materials can transform the electric energy into the mechanical energy and vice versa, and their performance is excellent in terms of frequency selectivity and frequency stability.

2. Design of electro-mechanical demultiplexer

2.1. Structure description

In this letter, the concept of electro-mechanical demultiplexer is proposed and realized based on piezoelectric metamaterials. In the proposed demultiplexer, the electro-mechanical waves of different frequencies can transmit along the respective routes and output from the corresponding channels, see Fig. 1b. The designed piezoelectric metamaterials have simple configurations, which are realized by integrating the periodic electrodes onto the surfaces of the homogeneous piezoelectric plates and connecting the top and the bottom electrodes with the external LC circuits, see Fig. 1a. The researches on such kind of piezoelectric phononic crystals or metamaterials indicate that their band structures can be tuned nondestructively by the external circuits [26–33]. Compared with the external circuits containing either the capacitors or the inductors only, the external circuits containing both the capacitors and the inductors (LC circuits) can control the resonance bandgaps of the symmetric Lamb waves propagating in the piezoelectric plates much more precisely, i.e. a resonance bandgap can be located in a specified frequency range by the adjustment of the LC circuits [34], which is an indispensable character of the piezoelectric plates for the present demultiplexer. The multi-channel demultiplexer can be obtained through the electric connection of several plates presented in Fig. 1b. For example, the 4-channel demultiplexer is composed of three piezoelectric plates I, II and III, which are connected by the wires, see Fig. 1b. In this letter, these three piezoelectric plates are supposed to be supported by a frame, which is much stiffer than the piezoelectric plates. And the corresponding support points can be regarded as the fixed points. In this way, the waves can hardly propagate from the piezoelectric plates into the frame, and the energy can only flow from the plate I into the plates II and III in an electric form.

Some regions of the plates connected with the same external LC circuits can be regarded as a finite piezoelectric metamaterial plate, which are labeled as P_A and P_B in Fig. 1a or P1–P6 in Fig. 1b. Each piezoelectric metamaterial plate is composed of *n* unit cells. The two finite metamaterial plates realized by using the same piezoelectric plate are connected by the input channel naturally, i.e. P1 and P2 for plate I, P3 and P4 for plate II and P5 and P6 for plate III. The distribution of the electrodes on each piezoelectric plate is symmetric with respect to the input channel in the middle. The energy is imported via the input channel and exported via the output channels on the two ends of each piezoelectric plate. The magnitudes of the inductances and the capacitances could be determined based on the analysis of the bandgaps of each metamaterial plate. The present electro-mechanical demultiplexer is a hierarchical structure, and the number of output channels can be increased or decreased by connecting or disconnecting the piezoelectric plates.

As in Ref. [35], the piezoelectric metamaterial plate is assumed to be made of PZ26 polarized along the thickness direction (x_3-direction) and covered by very thin periodic electrodes. The material parameters for PZ26 are $\rho = 7700$ kg/m^3, $c_{11} = 148$ GPa, $c_{13} = 85$ GPa, $c_{33} = 135$ GPa, $c_{44} = 28$ GPa, $e_{15} = 9.86$ C/m^2, $e_{31} = -2.8$ C/m^2, $e_{33} = 12.5$ C/m^2, $\varepsilon_{11} = 800 = 800\,\varepsilon_0$, $\varepsilon_{33} = 700 = 700\,\varepsilon_0$, where ε_0 is the vacuum permittivity. Thus, the mass and the stiffness of such electrodes are negligible. The unit cells are formed due to the periodic surface electrodes. The widths of the unit cell and the electrode are represented by w_u and w_e, respectively. The thickness of the piezoelectric plate is denoted by h. The length of the plate in the direction perpendicular to the $x_1 - x_3$ plane is l, which is assumed to be much larger than h. Thus, the piezoelectric plate is considered to be in the plane-strain state in our numerical simulation.

2.2. Bandgap analysis

The two-dimensional (2D) spectral element method (SEM) for the electro-elastic waves propagating in piezoelectric plates connecting with shunting circuits [34] is adopted to solve the problem under consideration, which is presented in Supplementary Material 1 (see Appendix A). The separate piezoelectric plates are connected by the wires via the electrodes. The two connected electrodes (a and b) have to satisfy the following electric conditions as

$$V_a = V_b, \quad D_a + D_b = 0, \tag{1}$$

where V_a, V_b and D_a, D_b are the electric potentials and the electric displacements, respectively.

Since the antisymmetric Lamb waves can be generated only by a voltage difference between the top and bottom plate surfaces, there is no coupling between the antisymmetric Lamb waves and the external circuits in our considered case. Thus, we only take the symmetric Lamb waves into account. Our design of the demultiplexer relies on the analysis of the corresponding bandgaps, which are obtained through the dispersion curves for the unit cell imposed by the Bloch–Floquet periodic boundary conditions. The high tunability of the bandgaps is necessary for our design. Therefore, the Bragg bandgaps are inappropriate for our purpose due to their low tenability [34–36], and only the bandgaps in the low-frequency region induced by the coupled resonance between the piezoelectric plate and the external circuits are considered here. The normalized frequency and wavenumber are defined as $\Omega = \omega w_u/\sqrt{c_{11}^*/\rho}$ and $\bar{k} = w_u/\lambda$, where the equivalent elastic constant for the thin plate is $c_{11}^* = c_{11}\left(1 - c_{13}^2/\left(c_{11}c_{33}\right)\right)$, with c_{11}, c_{13}, c_{33} being the elastic constants and ρ being the mass density of PZ26.

As a verification of the SEM, we also derived an analytical solution for the band structure of the unit cell based on the thin-plate assumption. For a thin piezoelectric plate, the electric field in the x_1-direction is assumed to disappear, which also leads to a zero electric displacement in the x_1-direction. In addition, the electric field along the thickness direction is assumed to be uniform. Thus, the governing equation can be reduced to

$$\frac{\partial^2 u_1}{\partial x^2} + \frac{\omega^2}{c^2}u_1 = 0, \tag{2}$$

where c is the wave velocity, which should be $\sqrt{c_{11}^*/\rho}$ for the part of the plate covered by the electrodes and $\sqrt{\bar{c}_{11}/\rho}$ for the part of the plate without electrodes, respectively, where $\bar{c}_{11} = c_f c_{11}^*$ with $c_f = \left(1 + k_{31}^{*\,2}\right)$ and $k_{31}^{*\,2} = \left(e_{31}^*\right)^2/c_{11}^*\varepsilon_{33}^*$. The detailed derivation for the analytical solution is provided in Supplementary Material 2 (see Appendix A).

In Fig. 3a, the influence of the thickness on the resonance bandgap is shown. The dispersion curves obtained by the SEM will approach the results obtained by the simplified thin-plate theory when the plate thickness becomes small, which therefore validates our numerical simulation.

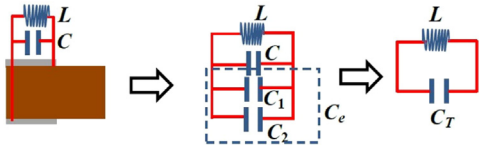

Fig. 2. The equivalent circuit. C_1 and C_2 represent the equivalent capacitances of the part covered by the electrodes and the rest uncovered part, respectively, $C_e = C_1 + C_2$ represents the total equivalent capacitance of the whole piezoelectric component, and C_T represents the total capacitance of the whole circuit (unit cell).

One outstanding characteristic of the proposed piezoelectric metamaterial plate in Fig. 1a is that the resonance frequency or the upper boundary of the resonance bandgap can be predicted approximately by the equivalent electric circuit as shown in Fig. 2. The piezoelectric component (the part of the plate within the unit cell) partly covered by the electrodes can be regarded as the parallel connection of two capacitors, where C_1 represents the equivalent capacitance of the part covered by the electrodes and C_2 represents the equivalent capacitance of the rest uncovered part [28]. Here, C_e is used to represent the total equivalent capacitance of the piezoelectric component, and $C_T = C + Ce$ represents the total capacitance of the whole circuit (unit cell). Thus, the resonance frequency can be calculated directly as

$$\omega_r = \frac{1}{\sqrt{LC_T}}, \tag{3}$$

It should be noted here that while C_1 can be evaluated analytically in the low-frequency or long-wavelength range [36], C_2 has to be determined numerically. In this study, the equivalent capacitance C_e of the whole piezoelectric component is determined directly in a numerical way. Specifically, the dispersion curves can be determined as shown in Fig. 3b when the magnitudes of L and C are given. The points marked by the crosses in Fig. 3b on the dispersion curves for the infinite wavelength ($\bar{k} \to 0$) lying above the upper boundaries of the resonance bandgaps are used to approximately evaluate the resonance frequency ω_r. Then, the value of C_e can be backwards calculated. For example, C_e is approximately $0.807C_0$ and $0.986C_0$ for $w_e/w_u = 1/2$ and 7/8, respectively. For convenience, the resonance frequency is normalized as $\bar{\omega}_r = 1/\sqrt{\bar{L}\bar{C}_T}$, where the dimensionless quantities are defined by $\bar{\omega}_r = \omega_r w_u/\sqrt{c_{11}^*/\rho}$, $\bar{C}_T = C_T/C_0$, $\bar{L} = L/L_0$, $C_0 = lw_u\varepsilon_{33}^*/h$, $L_0 = 1/C_0\omega_0^2$, and $\varepsilon_{33}^* = \varepsilon_{33}\left(1 + e_{33}^2/\left(\varepsilon_{33}c_{33}\right)\right)$ is the equivalent dielectric constant, e_{33} and ε_{33} are respectively the electro-elastic coupling coefficient and the dielectric constant, and ρ is the mass density of the plate.

2.3. Adjusting bandgaps by LC circuits

The more flat the dispersion curve lying above the resonance bandgap, the closer the upper boundary of the bandgap to the resonance frequency $\bar{\omega}_r$ (see Fig. 3b), the more accurate the prediction will be. Thus, the narrower electrodes are selected for the electro-mechanical demultiplexer as $w_e/w_u = 1/2$. The reason to select the LC circuits as the external circuits is that the resonance bandgaps in the low-frequency region can be tuned arbitrarily by the simultaneous adjustment of the inductors and the capacitors [34].

It means that the upper boundary and the width of the resonance bandgap can be tuned independently, see Fig. 3c. Specifically, the upper boundary of the resonance bandgap is adjusted

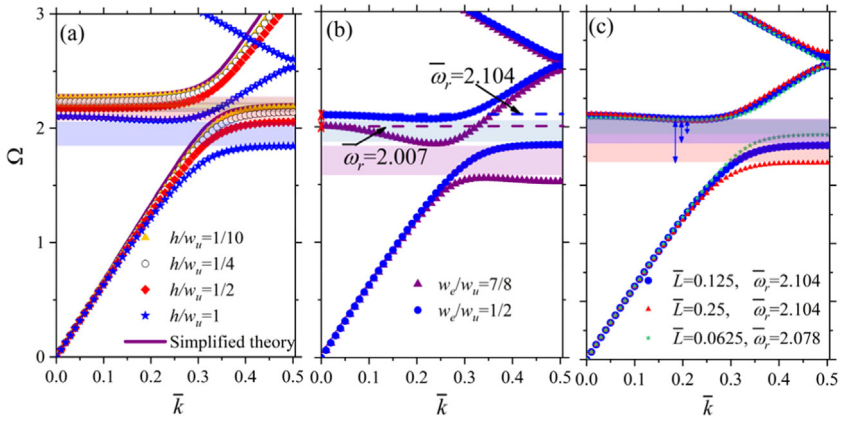

Fig. 3. The dispersion curves of the symmetric Lamb wave for the unit cell. (a) The influence of the plate thickness on the dispersion curves. (b) The influence of the electrode length on the dispersion curves. (c) The independent tunability of the bandwidth of the resonance bandgap. The parameters used in each figure are set as (a) $w_e/w_u = 1/2$, $\overline{L} = 0.125$, $\overline{C} = 1$, (b) $h/w_u = 1$, $\overline{L} = 0.125$, $\overline{C} = 1$, and (c) $w_e/w_u = 1/2$, $h = w_u$. The shadow areas represent the bandgaps.

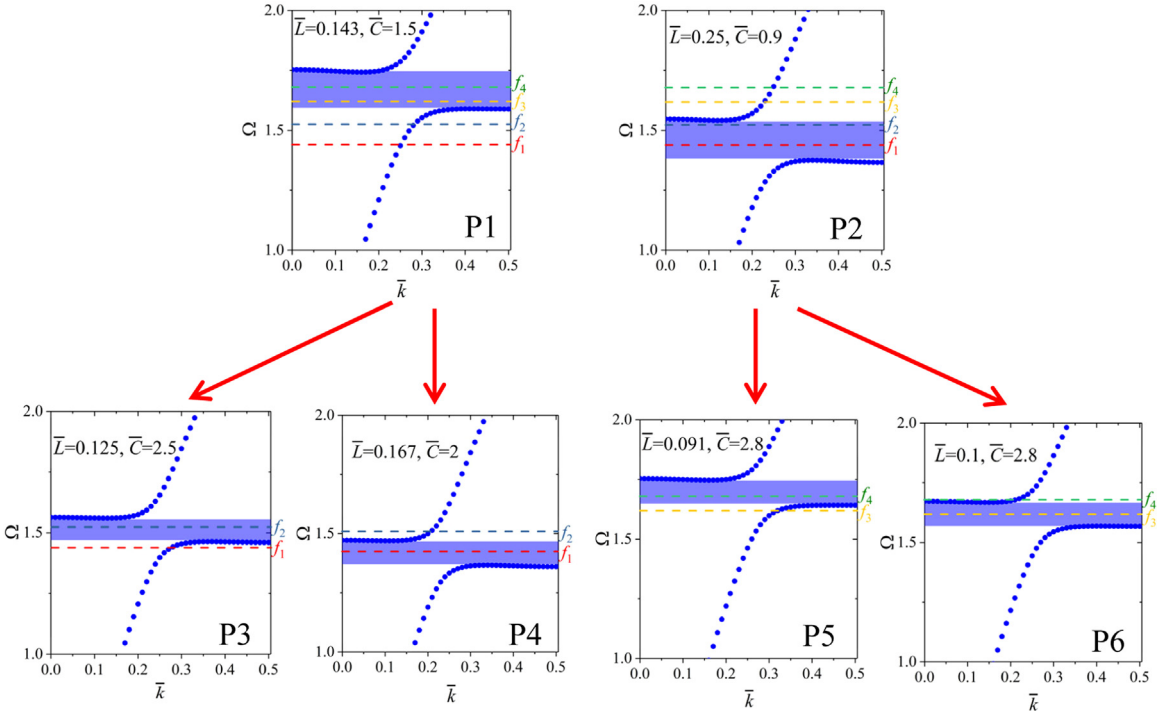

Fig. 4. The distributions of the resonance bandgaps for the piezoelectric metamaterial plates P1–P6 for the specified operating frequencies of the electro-mechanical demultiplexer.

to the target position firstly, and it can almost keep unchanged if we fix the resonance frequency $\overline{\omega}_r$. Then the bandwidth can be changed via the adjustment of the inductances. In some particular cases, however, the upper boundary may slightly deviate from the original position. In these cases, we need to fix the inductance while let the upper boundary move back to its original position by slightly changing the value of the resonance frequency $\overline{\omega}_r$. The target resonance bandgaps can be finally obtained by repeating these steps.

The design of the appropriate resonance bandgaps for the metamaterial plates P1–P6 is the most important step among the whole process. It is intended that the electro-mechanical wave with the specified frequency could transmit along the target path. It means that this wave should attenuate quickly on the other paths. An example is demonstrated to show how to determine the resonance bandgaps for each metamaterial plate when the operating frequencies of the electro-mechanical demultiplexer are chosen. It is assumed that the four operating frequencies are 395.828 kHz, 420.916 kHz, 451.578 kHz and 469.697 kHz, whose normalized values are calculated as $f_1 = 1.42$, $f_2 = 1.51$, $f_3 = 1.62$, $f_4 = 1.685$, respectively. And the electro-mechanical waves with the frequencies $f_1 - f_4$ are supposed to output from the channels 1–4, respectively. Thus, for the plate I, the resonance bandgaps of P1 and P2 should cover the frequencies f_3 and f_4 and the frequencies f_1 and f_2, respectively, see the top two figures in Fig. 4. In this way, the waves with the frequencies f_1 and f_2 and the waves with the frequencies f_3 and f_4 can transmit into the plate II and plate III, separately. Similarly, for plate II, the resonance bandgaps of P3 and P4 should cover the frequencies f_2 and f_1, respectively, see the first two figures on the bottom of Fig. 4. And for plate III, the resonance bandgaps of P5 and P6 should cover the frequencies f_4 and f_3, respectively, see the last two figures on the bottom of Fig. 4. The magnitudes of the inductances and the capacitances of the LC circuits for the

different metamaterial plates can be figured out when the desired resonance bandgaps are specified.

3. Device simulation

As a verification, a 2D numerical simulation is carried out for the 4-channel electro-mechanical demultiplexer described in Fig. 1b in the frequency domain. Referring to the experimental sample in the Ref. [35], the length and the thickness of the unit cells are both selected as 2 mm and each piezoelectric plate (I–III) is composed of 41 unit cells. Thus, each partial metamaterial plate (P1–P6) contains 19 unit cells. The input cell is fully covered by the electrodes and the rest cells are partly covered by the electrodes and the width of the electrodes is 1 mm, see Fig. 1a. The input signal is a voltage ($V_I = 200$ V), which is applied on the top electrode in the middle of plate I. And the corresponding bottom electrode is grounded. The voltages are applied at the four different frequencies $f_1 - f_4$, respectively. It should be pointed out that the symmetric boundary supports have practically no influences on the bandgaps of the symmetric Lamb waves. The distribution of the logarithm of the displacement field $G = 20\mathrm{Log}_{10}u$ in the 4-channel electro-mechanical demultiplexer is plotted in Fig. 5a for the four specified frequencies. It shows clearly that the waves with the different frequencies transmit along the different paths and finally output from the different channels. In Fig. 5b, the variations of the output voltages with the normalized frequency for the different channels are presented. The output voltage is normalized by the input voltage as $G = 20\mathrm{Log}_{10}(V_o/V_I)$. The bandgaps for the different output channels shown in Fig. 5b agree well with the corresponding bandgaps in Fig. 4, which justifies the validity of the present numerical calculations. In addition, Fig. 5b shows that the waves can propagate along the target paths while attenuate quickly along the other paths. It is shown that the voltage at the specified frequency output from each target channel is much higher than the voltages at the other frequencies in the same channel by 100 dB approximately. Thus, we can conclude that the effect of the crosstalk between the different outputs is very small and negligible for the proposed electro-mechanical demultiplexer.

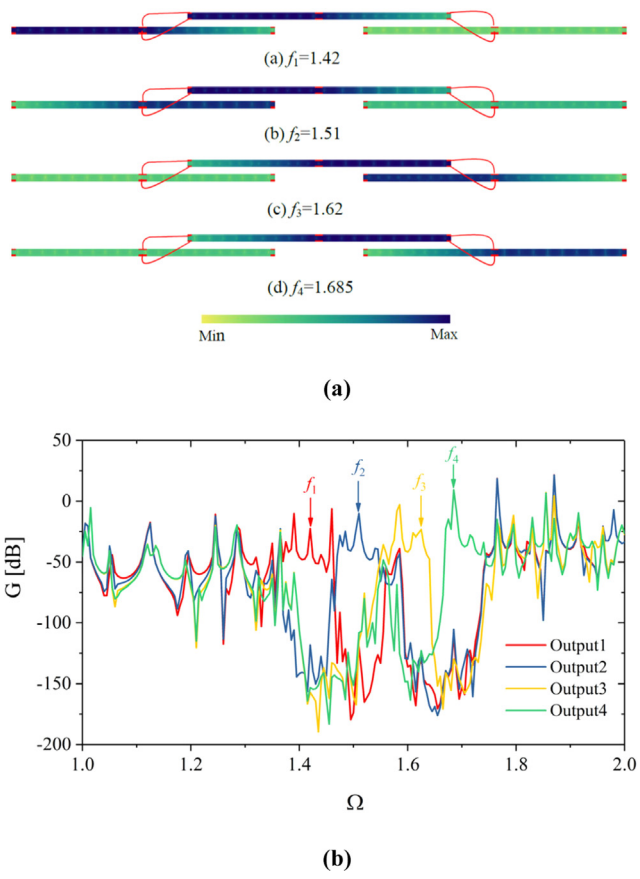

Fig. 5. The transmission of electro-mechanical waves in the 4-channel electro-mechanical demultiplexer. (a) The logarithm of the displacement field $G = 20\mathrm{Log}_{10}u$ of the electro-mechanical demultiplexer operating at the specified frequencies, (b) the variations of the output voltage $G = 20\mathrm{Log}_{10}(V_o/V_I)$ with the normalized frequency for the different output channels.

4. Conclusions

In summary, the first electro-mechanical demultiplexer is proposed and realized in this letter based on the novel piezoelectric metamaterial plate in a simple configuration. The independent tunabilities of the upper boundary and the bandwidth of the corresponding resonance bandgaps are indispensable for our design. The feasibility of the 4-channel electro-mechanical demultiplexer is confirmed by a numerical simulation. The present electro-mechanical demultiplexer has the following four outstanding characteristics:

- **The simple structure:** The whole model is only composed of several homogeneous piezoelectric plates. The piezoelectric metamaterial plate is covered by an array of periodic electrodes connected by the external LC circuits, and the different piezoelectric plates are connected electrically.
- **The high tunability:** The working frequencies can be changed at will and nondestructively via the adjustment of the external LC circuits. The number of the output channels can be easily increased or decreased by connecting or disconnecting the piezoelectric plates.
- **The excellent working performance:** The electro-mechanical waves with different frequencies can be split efficiently and the effect of the crosstalk between the different outputs is very small.
- **The electro-mechanical coupling:** The electro-mechanical demultiplexer has the potential to be integrated into some electrical devices just like crystal filters, which may promote the application of the acoustic/elastic demultiplexer in a wide range, such as wireless telecommunication and electric signal processing.

Declaration of competing interest

The authors declare that they have no known competing financial interests or personal relationships that could have appeared to influence the work reported in this paper.

Acknowledgments

This work is supported by the German Research Foundation (DFG, No. ZH 15/29-1), the Natural Science Foundation of Zhejiang Province (No. LD21A020001) and the Russian Foundation for Basic Research (No. 19-41-230012), which are gratefully acknowledged.

Appendix A. Supplementary data

Supplementary material related to this article can be found online at https://doi.org/10.1016/j.eml.2022.101610.

References

[1] S.A. Cummer, J. Christensen, A. Alù, Controlling sound with acoustic metamaterials, Nat. Rev. Mater. 1 (3) (2016) 1–13.

[2] Y. Chen, J. Hu, G. Huang, A design of active elastic metamaterials for control of flexural waves using the transformation method, J. Intell. Mater. Syst. Struct. 27 (10) (2016) 1337–1347.

[3] M. Ke, Z. Liu, C. Qiu, W. Wang, J. Shi, W. Wen, P. Sheng, Negative-refraction imaging with two-dimensional phononic crystals, Phys. Rev. B 72 (6) (2005) 064306.

[4] X. Li, X. Ni, L. Feng, M. Lu, C. He, Y. Chen, Tunable unidirectional sound propagation through a sonic-crystal-based acoustic diode, Phys. Rev. Lett. 106 (8) (2011) 084301.

[5] X. Zhou, M. Badreddine Assouar, M. Oudich, Acoustic superfocusing by solid phononic crystals, Appl. Phys. Lett. 105 (23) (2014) 233506.

[6] B. Rostami-Dogolsara, M.K. Moravvej-Farshi, F. Nazari, Acoustic add-drop filters based on phononic crystal ring resonators, Phys. Rev. B 93 (1) (2016) 014304.

[7] Y. Chen, R. Zhu, M.V. Barnhart, G. Huang, Enhanced flexural wave sensing by adaptive gradient-index metamaterials, Sci. Rep. 6 (1) (2016) 1–11.

[8] J.O. Vasseur, P.A. Deymier, B. Djafari-Rouhani, Y. Pennec, A.C. Hladky-Hennion, Absolute forbidden bands and waveguiding in two-dimensional phononic crystal plates, Phys. Rev. B 77 (8) (2008) 085415.

[9] X. Zhang, Z. Liu, Superlenses to overcome the diffraction limit, Nature Mater. 7 (6) (2008) 435–441.

[10] S.A. Cummer, B.I. Popa, D. Schurig, D.R. Smith, J. Pendry, M. Rahm, A. Starr, Scattering theory derivation of a 3D acoustic cloaking shell, Phys. Rev. Lett. 100 (2) (2008) 024301.

[11] N. Gao, J. Li, R. Bao, W. Chen, Harnessing uniaxial tension to tune Poisson's ratio and wave propagation in soft porous phononic crystals: An experimental study, Soft Matter 15 (14) (2019) 2921–2927.

[12] K. Bertoldi, M.C. Boyce, Wave propagation and instabilities in monolithic and periodically structured elastomeric materials undergoing large deformations, Phys. Rev. B 78 (18) (2008) 184107.

[13] L. Airoldi, M. Ruzzene, Design of tunable acoustic metamaterials through periodic arrays of resonant shunted piezos, New J. Phys. 13 (11) (2011) 113010.

[14] E.A. Flores Parra, A. Bergamini, B. Lossouarn, B.V. Damme, M. Cenedese, P. Ermanni, Bandgap control with local and interconnected LC piezoelectric shunts, Appl. Phys. Lett. 111 (11) (2017) 111902.

[15] J.F. Robillard, O.B. Matar, J.O. Vasseur, P.A. Deymier, M. Stippinger, A.C. Hladky-Hennion, Y. Pennec, B. Djafari-Rouhani, Tunable magnetoelastic phononic crystals, Appl. Phys. Lett. 95 (12) (2009) 124104.

[16] Y. Pennec, B. Djafari-Rouhani, J.O. Vasseur, A. Khelif, P.A. Deymier, Tunable filtering and demultiplexing in phononic crystals with hollow cylinders, Phys. Rev. E 69 (4) (2004) 046608.

[17] B. Rostami-Dogolsara, M.K. Moravvej-Farshi, F. Nazari, Designing switchable phononic crystal-based acoustic demultiplexer, IEEE Trans. Ultrason. Ferroelectr. Freq. Control 63 (9) (2016) 1468–1473.

[18] Q. Zou, W. Liu, T. Yu, N. Liu, T. Wang, Q. Liao, Decoupling of multiple coupled phononic crystal waveguides: Application to acoustic demultiplexing, J. Phys. D: Appl. Phys. 50 (12) (2017) 125102.

[19] P. Moradi, A. Bahrami, Three channel GHz-ranged demultiplexer in solid–solid phononic crystals, Chin. J. Phys. 59 (2019) 291–297.

[20] F. Motaei, A. Bahrami, Eight-channel acoustic demultiplexer based on solid-fluid phononic crystals with hollow cylinders, Photon. Nanostruct. Fundam. Appl. 39 (2020) 100765.

[21] A.A. Watkins, O.R. Bilal, Demultiplexing infrasound phonons with tunable magnetic lattices, Front. Mater. 7 (2020) 410.

[22] O.R. Bilal, C.H. Yee, J. Rys, C. Schumacher, C. Daraio, Experimental realization of phonon demultiplexing in three-dimensions, Appl. Phys. Lett. 118 (9) (2021) 091901.

[23] W.P. Mason, Electrical wave filters employing quartz crystals as elements, Bell Syst. Tech. J. 13 (3) (1934) 405–452.

[24] R.G. Kinsman, A history of crystal filters, in: Proceedings of the 1998 IEEE International Frequency Control Symposium, 1998, pp. 563–570.

[25] C.C. Ruppel, Acoustic wave filter technology - A review, IEEE Trans. Ultrason. Ferroelectr. Freq. Control 64 (9) (2017) 1390–1400.

[26] N. Kherraz, L. Haumesser, F. Levassort, P. Benard, B. Morvan, Controlling Bragg gaps induced by electric boundary conditions in phononic piezoelectric plates, Appl. Phys. Lett. 108 (9) (2016) 093503.

[27] C.J. Rupp, M.L. Dunn, K. Maute, Switchable phononic wave filtering, guiding, harvesting, and actuating in polarization-patterned piezoelectric solids, Appl. Phys. Lett. 96 (11) (2010) 111902.

[28] N. Kherraz, L. Haumesser, F. Levassort, P. Benard, B. Morvan, Hybridization bandgap induced by an electrical resonance in piezoelectric metamaterial plates, J. Appl. Phys. 123 (9) (2018) 094901.

[29] C. Vasseur, C. Croënne, J.O. Vasseur, B. Dubus, M. Pham Thi, C. Prévot, A.C. Hladky-Hennion, Electrical evidence of the tunable electrical Bragg bandgaps in piezoelectric plates, IEEE Trans. Ultrason. Ferroelectr. Freq. Control 65 (9) (2018) 1552–1562.

[30] N. Kherraz, F.H. Chikh-Bled, R. Sainidou, B. Morvan, P. Rembert, Tunable phononic structures using lamb waves in a piezoceramic plate, Phys. Rev. B 99 (9) (2019) 094302.

[31] P. Chen, Y.Z. Wang, Y.S. Wang, Active control of flexural waves in a phononic crystal beam with staggered periodic properties, Wave Motion 93 (2020) 102481.

[32] L. Ning, Y.Z. Wang, Y.S. Wang, Active control cloak of the elastic wave metamaterial, Int. J. Solids Struct. 202 (2020) 126–135.

[33] L. Ning, Y.Z. Wang, Y.S. Wang, Active control of a black hole or concentrator for flexural waves in an elastic metamaterial plate, Mech. Mater. 142 (2020) 103300.

[34] Y. Wang, C. Zhang, W. Chen, Z. Li, M.V. Golub, S.I. Fomenko, Precise and target-oriented control of the low-frequency lamb wave bandgaps, J. Sound Vib. 511 (2021) 116367.

[35] F.H. Chikh-Bled, N. Kherraz, R. Sainidou, P. Rembert, B. Morvan, Piezoelectric phononic plates: Retrieving the frequency band structure via all-electric experiments, Smart Mater. Struct. 28 (11) (2019) 115046.

[36] C. Vasseur, C. Croënne, J.O. Vasseur, B. Dubus, M. Pham Thi, C. Prévot, A.C. Hladky-Hennion, Electrical evidence of the tunable electrical bragg bandgaps in piezoelectric plates, IEEE Trans. Ultrason. Ferroelectr. Freq. Control 65 (9) (2018) 1552–1562.